Cement and Concrete Research 41 (2011) 107–112

Contents lists available at ScienceDirect

Cement and Concrete Research

journal homepage: http://ees.elsevier.com/CEMCON/default.asp

# Bulk modulus of basic sodalite, $Na_8[AlSiO_4]_6(OH)_2 \cdot 2H_2O$, a possible zeolitic precursor in coal-fly-ash-based geopolymers

Jae Eun Oh [a], Juhyuk Moon [a], Mauricio Mancio [a], Simon M. Clark [b,c], Paulo J.M. Monteiro [a,*]

[a] Department of Civil and Environmental Engineering, University of California, Berkeley, CA 94720, USA
[b] Advanced Light Source, Lawrence Berkeley National Laboratory, Berkeley, CA 20015, USA
[c] Department of Earth and Planetary Sciences, University of California, Berkeley, CA 94720, USA

ARTICLE INFO

*Article history:*
Received 10 March 2010
Accepted 24 September 2010

*Keywords:*
Geopolymer
Fly ash
Basic sodalite
Bulk modulus
High pressure

ABSTRACT

Synthetic basic sodalite, $Na_8[AlSiO_4]_6(OH)_2 \cdot 2H_2O$, cubic, P43n, (also known as hydroxysodalite hydrate) was prepared by the alkaline activation of amorphous aluminosilicate glass, obtained from the phase separation of Class F fly ash. The sample was subjected to a process similar to geopolymerization, using high concentrations of a NaOH solution at 90 °C for 24 hours. Basic sodalite was chosen as a representative analogue of the zeolite precursor existing in Na-based Class F fly ash geopolymers. To determine its bulk modulus, high-pressure synchrotron X-ray powder diffraction was applied using a diamond anvil cell (DAC) up to a pressure of 4.5 GPa. A curve-fit with a truncated third-order Birch–Murnaghan equation of state with a fixed $K'_o = 4$ to pressure-normalized volume data yielded the isothermal bulk modulus, $K_o = 43 \pm 4$ GPa, indicating that basic sodalite is more compressible than sodalite, possibly due to a difference in interactions between the framework host and the guest molecules.



## 1. Introduction

Engineering the recycling of coal fly ash for use in cement and concrete manufacturing has been studied extensively and continues to be an active area of research [1–3]. Although its incorporation into cementitious materials is on the rise, a large amount of fly ash is still disposed of into landfills or deposited in the ocean. In 2004 in the United States, according to the American Coal Ash Association (ACAA) [4], 70.8 million tons of coal fly ash was produced and 42.7 million tons of that coal fly ash was disposed into the ground or ocean. In 2007 in Europe (EU 15), 41 million tons of coal fly ash was generated, with a reutilization rate of only 47% [5]. As the cost of disposing of fly ash continues to rise, strategies for the recycling of fly ash is environmentally and economically critical. The geopolymer science and zeolite synthesis fields that use fly ash as source materials are two emerging areas for the recycling of coal fly ash [6,7]. Interestingly, the science of zeolite formation using fly ash has been regarded as an analogue of fly-ash-based geopolymer synthesis in terms of synthesis methodologies [8].

The reaction product of geopolymerization is, clearly, the zeolite precursor [9]. The similarities in terms of their nanostructure between zeolites and geopolymers synthesized from coal fly ash have been discussed in earlier studies [10,11]. Provis et al. [12] suggested the widespread existence of nanocrystalline-size zeolites with no more than four unit cells, which corresponded to approximately 8–10 nm as the main phase, resulting in the broad ~28° peak of characteristic in the X-ray diffraction pattern of geopolymer. Table 1 presents the most frequently observed crystalline zeolitic phases in geopolymer studies. Zeolites belonging to the "ABC-6 family" framework were often found when Class F fly ash was activated by a high concentration of a NaOH (or a mixture with Na-silicate) solution (>5~8 M) [6], which is a strong geopolymerization activator. These zeolites include hydroxysodalite, herschelite (=Na-chabazite), nepheline, and hydroxycancrinite. Other types of zeolites not belonging to the ABC-6 family (e.g., zeolite Na-P1, analcime) were also observed in geopolymers; however, these zeolite usually formed when a low concentration of NaOH solution (< 2~3 M) was used [6]; this is a weak geopolymerization activator. This observation seems to indicate that the geopolymer reaction product, also called the zeolitic precursor, possess a similar structure as the ABC-6 family of zeolite minerals when a high concentration of Na-based alkali-activating solution is used [7]. This hypothesis is also supported by the observation that the $^{29}Si$ NMR spectrum of aged fly ash geopolymers is identical to herschelite [13].

The framework of ABC-6 family zeolites, known as a "six-membered ring", consists of Al- and Si-tetrahedra. Only nineteen members of zeolite framework types are categorized as ABC-6 family among the known 176 zeolite framework types. The main difference between zeolites belonging to the ABC-6 family is only in the stacking sequence of the six-membered rings [14]. Of the zeolitic materials belonging to the ABC-6 family framework type, hydroxysodalite and hydroxycancrinite were suggested as the best candidates to represent the structure of a zeolitic precursor [7] and to play a similar function as the role that 14 Å tobermorite and jennite play in C–S–H in cement science.

* Corresponding author.
*E-mail address:* monteiro@berkeley.edu (P.J.M. Monteiro).

0008-8846/$ – see front matter © 2010 Elsevier Ltd. All rights reserved.
doi:10.1016/j.cemconres.2010.09.012

**Table 1**
Crystalline zeolite phases of geopolymers in the literature.

| Reference | Crystalline phases | Material and activator |
|---|---|---|
| Palomo et al. (1999) [9] | Hydroxysodalite | Class F fly ash, NaOH, Na-silicate |
| Krivenko and Kovalchuk (2002) [15] | Hydroxysodalite, analcime | Class F fly ash, NaOH, Na-silicate |
| Criado et al. (2005) [16] | Hydroxysodalite, Na-chabazite (=herschelite), sodium bicarbonate | Class F fly ash, NaOH, Na-silicate |
| Bakharev (2005) [17] | Hydroxysodalite, chabazite, zeolite Na-P1 | Class F fly ash, NaOH, Na-silicate |
| Bakharev (2005) [18] | Hydroxysodalite, trace of chabazite, zeolite Na-P1, zeolite A | Class F fly ash, NaOH, Na-silicate |
| Fernandez-Jimenez et al. (2005) [19] | Hydroxysodalite, herschelite-type mineral | Class F fly ash, NaOH |
| Bakharev (2006) [20] | Hydroxysodalite, nepheline, zeolite Na-P1 | Class F fly ash, NaOH, KOH, Na-silicate |
| Criado et al. (2007) [21] | Sodalite, Na-chabazite, zeolite P(Na), zeolite Y (=faujasite variant) | Class F fly ash, NaOH, Na-silicate |
| Dombrowski et al. (2007) [22] | Sodalite, nepheline | Class F fly ash, NaOH, Ca(OH)2 |
| Fernandez-Jimenez et al. (2007) [23] | Hydroxysodalite, Na-chabazite (=herschelite), analcime | Class F fly ash, NaOH, Na-silicate |
| Alvarez-Ayuso et al. (2008) [24] | Sodalite, chabazite, faujasite, zeolite Na-P1, zeolite 4A (=zeolite A) | Class F fly ash, NaOH |
| J. Oh et al. (2010) [7] | Hydroxycancrinite, hydrotalcite | Class F fly ash, NaOH |

Wide presence of hydroxysodalite has been often reported by geopolymer researchers from the geopolymer matrices synthesized using Class F coal fly ashes with high NaOH concentrated solution (see Table 1); however, it is highly probable that what their studies were actually seeing was basic sodalite [25], given that hydroxysodalite must be obtained through thermal drying treatment (e.g., 3 hours at ~873 K under vacuum or $N_2$ atmosphere condition [26,27]). Care should be taken in distinguishing between hydroxysodalite and basic sodalite. Although both of them are structurally very similar and belong to the same structural zeolitic material group—called the "hydrosodalite" group—they are slightly different in chemical composition.

The aluminosilicate minerals of the hydrosodalite group are expressed in a general chemical formula: $Na_{6+x}[AlSiO_4]_6(OH)_x \cdot nH_2O$ ($x=0,2$ and $n=0$ to 2) [25]. Here, the sodalite β-cage frame is indicated by $[AlSiO_4]_6^{6-}$, which forms the sodalite framework. Other non-framework components, such as cation $Na^+$, anion $OH^-$, and $H_2O$, are contained in the β-cages of the structure. The sodalite framework structure is shown in Fig. 1. Earlier hydrothermal zeolite studies synthesized different compositions of hydrosodalite group minerals, which were divided into two groups: (1) the "basic" hydrosodalite, $Na_8[AlSiO_4]_6(OH)_2 \cdot 2H_2O$, also known as "basic sodalite" [28] or "hydroxysodalite hydrate" [29] and (2) the "non-basic" hydrosodalite, $Na_6[AlSiO_4]_6 \cdot 8H_2O$, also called "hydrosodalite" [25]. Interestingly, all mineral members belonging to the hydrosodalite group have the same cubic symmetry, with a space group of $P\bar{4}3n$. The hydroxysodalite, $Na_8[AlSiO_4]_6(OH)_2$ (case of $x=2$ and $n=0$), is the dehydrated form of basic sodalite [27].

Despite large advances in the understanding of geopolymers in general, little is known about the mechanical properties of geopolymer at an atomic level. The current study determined the bulk modulus—one of the fundamental mechanical properties of materials—of basic sodalite using high-pressure synchrotron X-ray diffraction.

## 2. Experimental procedure

The source material for the tested sample was an aluminosilicate glass that was separated from a Class F fly ash by using the density difference of the constituents. The original Class F fly ash was mixed into a mixture solution containing deionized water and 30 ml/l calgon [5% sodium hexametaphosphate, $(NaPO_3)_6$, used as a deflocculant], in a 2-liter beaker, with a solid-to-liquid ratio of 100 g/l. After settling for 20 minutes, the solution with suspended particles was siphoned out and centrifuged for 20 minutes at 20,000 rpm. After centrifugation, water was removed and the remaining material, consisting of the separated amorphous phase, was dried in an oven at 105 °C. The chemical composition of the aluminosilicate glass before alkaline activation is given in Table 2. Then, 10 *g* of solid aluminosilicate glass powder was mixed with 10 ml of 10 M NaOH solution. The solution mixture was heated at 90 °C for 24 hours in a water bath, which was used in our previous geopolymer study [7]. After being subjected to heat for 24 hours, the sample was examined by synchrotron X-ray diffraction to identify the basic sodalite phase.

Phase identification of the synthesized phases and high-pressure powder X-ray diffraction were carried out at beamline 12.2.2 of the Advanced Light Source [30] using a synchrotron monochromatic X-ray beam with $\lambda = 0.6199$ Å (=20 keV energy). The National Bureau of Standards $LaB_6$ Powder Diffraction Standard was used to calibrate the working distance between the samples and the detector. Diffraction patterns were collected at room temperature using a MAR345 image plate (3450 × 3450 pixels), with an exposure time of 600 seconds and analyzed with the FIT2D [31], XFIT [32], and Celref [33] software programs.

The alkali-activated sample was finely ground and mixed with a pressure medium liquid (4:1 volume ratio of a methanol/ethanol solution) and housed in a sample chamber drilled in a steel gasket in a diamond anvil cell (DAC). The chamber was 180 μm in diameter, with a

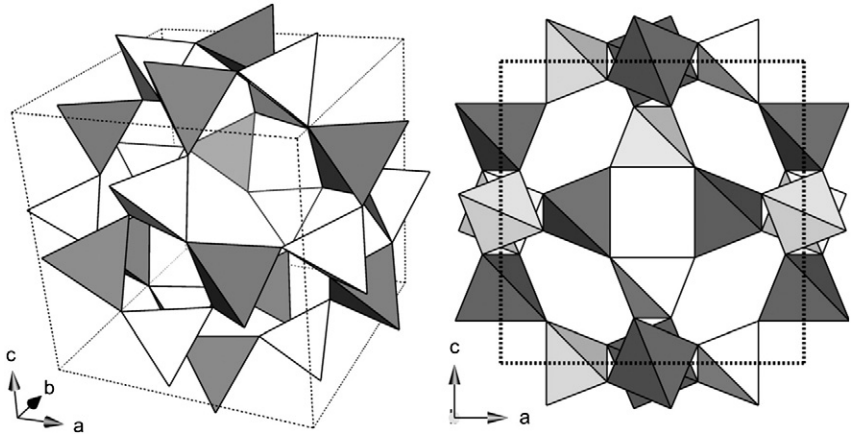


**Fig. 1.** Sodalite framework structure (SOD), of which hydroxysodalite and the basic sodalite belong to. The dark tetrahedra indicate Al-tetrahedra and the light ones show Si-tetrahedra.

**Table 2**
Chemical composition (weight%) of the raw material before alkaline activation; aluminosilicate glass separated from Class F coal fly ash.

| Chemical composition (wt.%) | |
|---|---|
| $SiO_2$ | 45.10 |
| $Al_2O_3$ | 21.36 |
| $Fe_2O_3$ | 4.81 |
| $K_2O$ | 1.47 |
| $TiO_2$ | 1.02 |
| CaO | 8.74 |
| $Na_2O$ | 5.19 |
| $SO_3$ | 5.19 |
| MgO | 3.49 |
| MnO | 0.09 |
| LOI | 3.54 |

75-μm thickness. The pressure inside the chamber was measured using the ruby [$Al_2O_3$ doped with $Cr^{3+}$ (0.05%)] fluorescence calibration method [34] and was increased up to 4.5 GPa in a hydrostatic condition.

The high-pressure X-ray diffraction technique using a diamond anvil cell uses crystallographic information to obtain the bulk modulus of materials. This technique is especially suitable here because it excludes all undesirable effects of impurities, such as unreacted mineral components of fly ashes, which might be present in the samples. The bulk modulus was calculated from the unit cell volume contraction under high pressure.

## 3. Result and discussion

Fig. 2 shows the synchrotron X-ray powder diffraction pattern for the sample. The major synthesized crystalline phases were identified as C–S–H(I) (JCPDS card # 01-0010) and basic sodalite (JCPDS card # 11-0401; see Fig. 2). The amorphous hump appearing around the *d*-spacing of 2~4.5 Å indicates geopolymer formation [7,16,21]. The quantification of the reaction products by X-ray diffraction Rietveld refinement is difficult because currently there is no complete atomic structure information for the geopolymer (= amorphous hump) and C–S–H(I) (i.e., no CIF file exists); however, the approximate weight% of the reaction products can be estimated when the C–S–H(I) structure is assumed to be similar to that of the 14-Å tobermorite and the refinement is limited only to crystalline phases. The refinement result indicates that the basic sodalite phase takes up approximately ~70%; C–S–H(I), ~24%; hydrotalcite, ~4%; and quartz, ~1% in all crystalline phases (the results were obtained from the software MAUD [35]). Since the geopolymer formed in the current study is considered to have similar atomic structure to basic sodalite (e.g., in the form of nano-crystalline basic sodalite

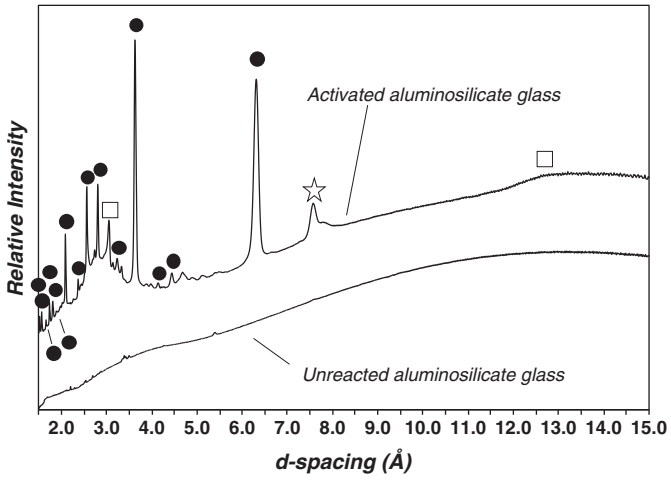


**Fig. 2.** X-ray diffractogram of powder sample made of activated aluminosilicate glass by alkaline activation for 24 hours at 90 °C. ●: basic sodalite, □: C–S–H (I) and ☆: hydrotalcite.

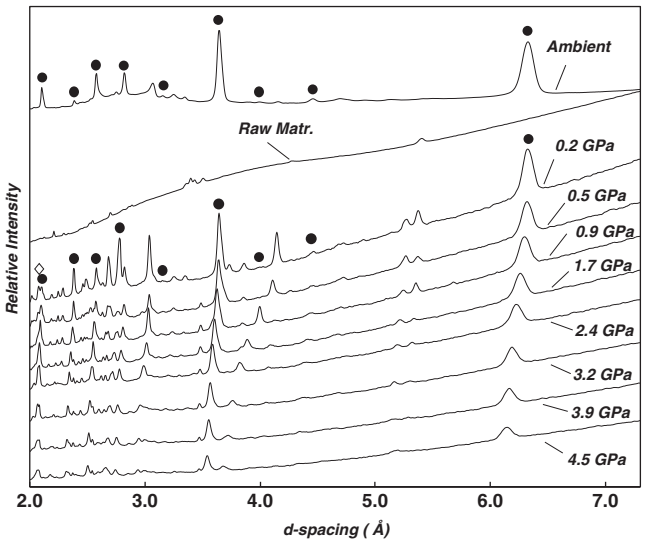


**Fig. 3.** Integrated powder X-ray diffraction patterns of synthetic basic sodalite as a function of pressure, where the pattern with a label of "RawMatr." was taken from the aluminosilicate glass phase of Class F fly ash at ambient conditions. The labels imply as follows: ● = basic sodalite and ◇ = diamond.

according to Provis et al. [12]), the weight% of the basic sodalite may be more than 70% in the sample.

As expected, all *d*-spacings of the observed diffraction peaks of basic sodalite appeared slightly larger than the hydroxysodalite found in the literature (JCPDS card #11-0401), indicating that the unit cell dimension of the basic sodalite is slightly expanded compared to hydroxysodalite due to extra water molecules [36].

Fig. 3 illustrates the profiles of one-dimensional integrated powder X-ray diffraction patterns under high pressure, which shows no separation or merging of diffracted peaks of the basic sodalite, demonstrating that the high pressure application did not change the symmetry of the basic sodalite. Changes in lattice parameter and unit cell volume of the basic sodalite under high pressure were calculated using the Celref software (unit cell refinement software; see Table 3) and the normalized values are depicted in Fig. 4. No discontinuity in the $P$–$(V/V_o)$ plot was observed in the measured pressure range.

The pressure-normalized volume data below 4.5 GPa was fitted by a third-order Birch–Murnaghan equation of state (B–M EoS) [37–39]. In the curve-fitting, the third-order Birch–Murnaghan equation of state is reorganized into the simpler linear form: $F(f) = K_o - 1.5K_o(4 - K_o')f$ by defining the normalized pressure parameter $F = P/\{1.5[(V/V_o)^{-7/3} - (V/V_o)^{-5/3}]\}$ and the Eulerian strain parameter $f = 0.5[(V/V_o)^{-2/3} - 1]$. In the plot of $F$ versus $f$, the $y$-intercept and the slope of the weighted least-squares fit gave the bulk modulus $K_o$ and its derivative $K_o'$ [37]. In this study, a weighted linear least-squares fit with errors was applied to the $f$–$F$ plot to reduce any erroneous effects from measurement errors [40]. The bulk modulus of the basic sodalite was calculated as $K_o = 43 \pm 4$ GPa, as

**Table 3**
Unit cell lattice parameters and volume for the basic sodalite under hydrostatic pressure. The basic sodalite consists of a cubic system with a space group of $P\bar{4}3n$.

| Pressure (GPa) | Unit Cell Volume (Å$^3$) | Lattice Parameters a(Å) |
|---|---|---|
| 0.0 ± 0.0 | 707 ± 3 | 8.91 ± 0.012 |
| 0.2 ± 0.1 | 705 ± 3 | 8.90 ± 0.012 |
| 0.5 ± 0.1 | 703 ± 3 | 8.89 ± 0.015 |
| 0.9 ± 0.2 | 694 ± 4 | 8.85 ± 0.015 |
| 1.7 ± 0.2 | 684 ± 3 | 8.81 ± 0.011 |
| 2.4 ± 0.2 | 674 ± 4 | 8.77 ± 0.018 |
| 3.2 ± 0.3 | 661 ± 2 | 8.71 ± 0.011 |
| 3.9 ± 0.3 | 655 ± 2 | 8.683 ± 0.009 |
| 4.5 ± 0.4 | 648 ± 2 | 8.655 ± 0.008 |

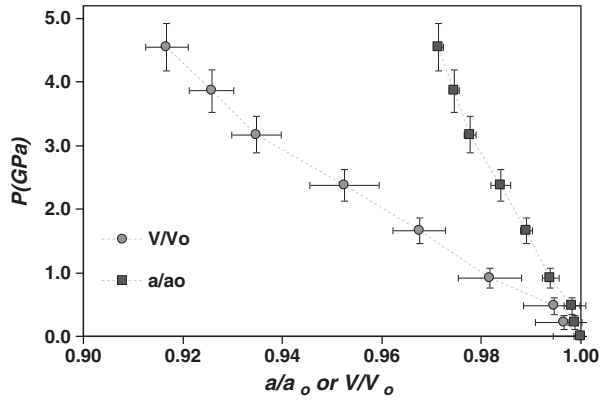


**Fig. 4.** Structural changes in normalized unit cell parameter and volume ratio of the basic sodalite under pressure.

shown in Fig. 5. Note: $K'_o$ was assumed to be 4 because the B–M EoS curve-fitting produced an unrealistic value of 0.1. A value close to 4 is standard in natural minerals and zeolites [41,42].

As illustrated in Fig. 6, earlier studies reported the bulk moduli of sodalite, $Na_8[AlSiO_4]_6Cl_2$, as possessing the same framework structure [43,44] as the basic sodalite. Hazen and Sharp [43] reported the bulk modulus of sodalite as $K_o = 52 \pm 8$ GPa ($K'_o = 4$, fixed) using a truncated Birch–Murnaghan equation of state (i.e., $K'_o$ was fixed as 4 in the curve-fitting); this value is relatively larger than that obtained

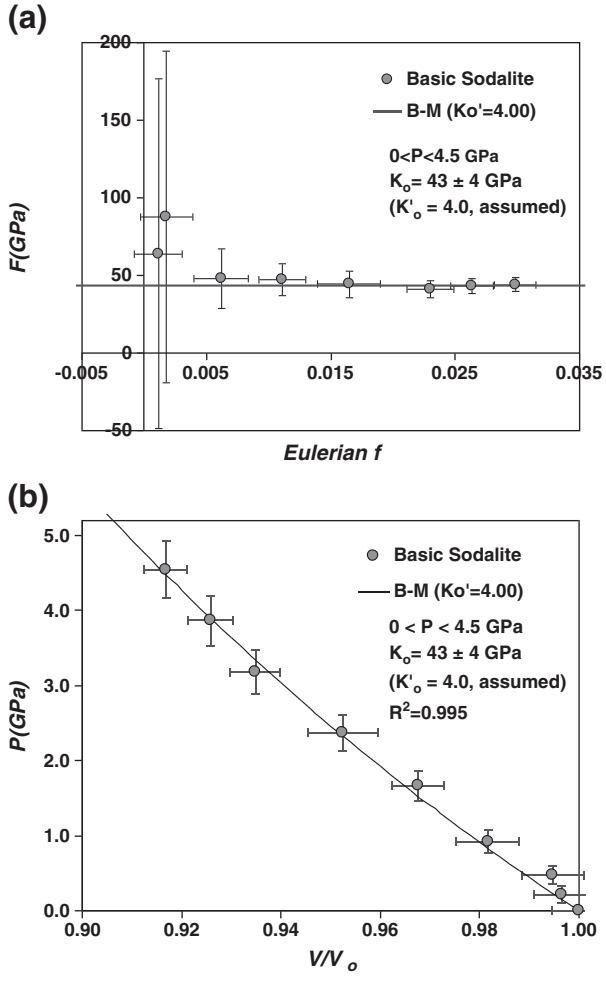


**Fig. 5.** (a) Plot of normalized pressure *F* versus Eulerian *f*. (b) Pressure-normalized volume data of the basic sodalite and its curve-fitting with third-order Birch–Murnaghan equation of state (solid line).

in the current study. Werner et al. [44] performed a single crystal sodalite high-pressure measurement of up to 7.4 GPa and claimed a possible phase transition or change of compression behavior based on their observation of the slope change of the *P*–*V* curve appearing at near 3 GPa, although there was no observed symmetry change of structure; any evidence of a phase transition or change in compressive behavior, however, was not observed in the current *P*-normalized *V* data. The authors calculated two separate bulk moduli for the single crystal sodalite in two different pressure ranges: $K_o = 49 \pm 6$ GPa for P<3 GPa and $K_o = 93 \pm 7$ GPa for P>3 GPa ($K'_o$ was not provided in the paper). By applying a single Birch–Murnaghan equation fitting for the entire pressure range, they also calculated the bulk modulus of $K_o = 37 \pm 3$ GPa with $K'_o = 15 \pm 2$. This value for $K'_o$ is too high to be realistic [41,42].

The current study reexamined the *P*–*V* data of Werner et al. by fixing $K'_o = 4$ (see Fig. 6), yielding a new value $K_o = 56 \pm 7$ GPa for the whole pressure range. Although the *P*–*V* curve trend of the basic sodalite in the current study resembles that of the previous study, the bulk modulus for the basic sodalite appears to be less than that of sodalite; This condition may be due to different bonding energies (or bonding angles), to the framework, of guest ions (i.e., $Cl^-$ for sodalite versus $OH^-$ and $H_2O$ for the basic sodalite) that are contained in the sodalite cage (i.e., different host–guest interaction). In general, the sodalite framework structure can be modified by a variety of host–guest interactions between the aluminosilicate framework and non-framework guest molecules, such as cations ($Li^+$, $Na^+$, and $K^+$), anions ($Cl^-$ and $OH^-$), or neutral molecules (e.g., $H_2O$), resulting in unit cell volume change [45]. The bond lengths of Al–O and Si–O of the sodalite framework structure should be constant, irrespective of the guest ions [46], and quite rigid so that the volume change of the unit cell is mainly governed by the tilting of $AlO_4$ or $SiO_4$ tetrahedra of the framework [45]; therefore, the larger the unit cell of sodalite, the more flexible the structure, resulting in a tendency to change geometrically under pressure (i.e., become more compressible). The unit cell volume of sodalite used in the current study (~707 $Å^3$) was larger than that of sodalite (~699.7 $Å^3$ [43]), a possible explanation for the higher compressibility of the basic sodalite. In addition, the disordered characteristic of guest molecules can also cause the higher compressibility of the basic sodalite. Wiebcke et al. [25] reported that the $OH^-$ ions and $H_2O$ molecules residing in the sodalite cage of basic sodalite do not exist individually, but appear in a single formation of $O_2H_3^-$, due to a very strong hydrogen bond between O and H, where the central H and O atoms possess dynamically disordered orientation, which might cause the basic sodalite to be less stable against the compression. They also found that there is no hydrogen bonding of the end $OH^-$ of $O_2H_3^-$ to the oxygen of the framework (i.e., there is no strong connection between the guest and the framework), which may support the first explanation of the geometrical flexibility of the basic sodalite framework structure.

The bulk modulus of helvite, $Mn_8[BeSiO_4]_6\,S_2$, which has also the sodalite framework with the same space group, is calculated in the current study using the high-pressure measurement data shown in study of Kudoh et al. [47] because they did not provide any calculation of bulk modulus. As seen in Fig. 6, the helvite, $K_o = 110 \pm 5$ GPa ($K'_o = 4$, fixed), appears much less compressible than the other sodalite framework materials, implying that the elemental composition of the framework structure is a more dominant factor than the topology of zeolite in determining the compression behavior of sodalite group zeolites, which would make the framework structure of helvite more rigid.

## 4. Conclusion

The current study chose the basic sodalite as a possible candidate representing the nanostructure of the zeolitic precursor of a Class F fly-ash-based geopolymer formed in high concentrations of a NaOH solution. A high-pressure synchrotron X-ray diffraction study computed a bulk modulus of the basic sodalite as $K_o = 43 \pm 4$ GPa (assuming $K'_o = 4.0$). No

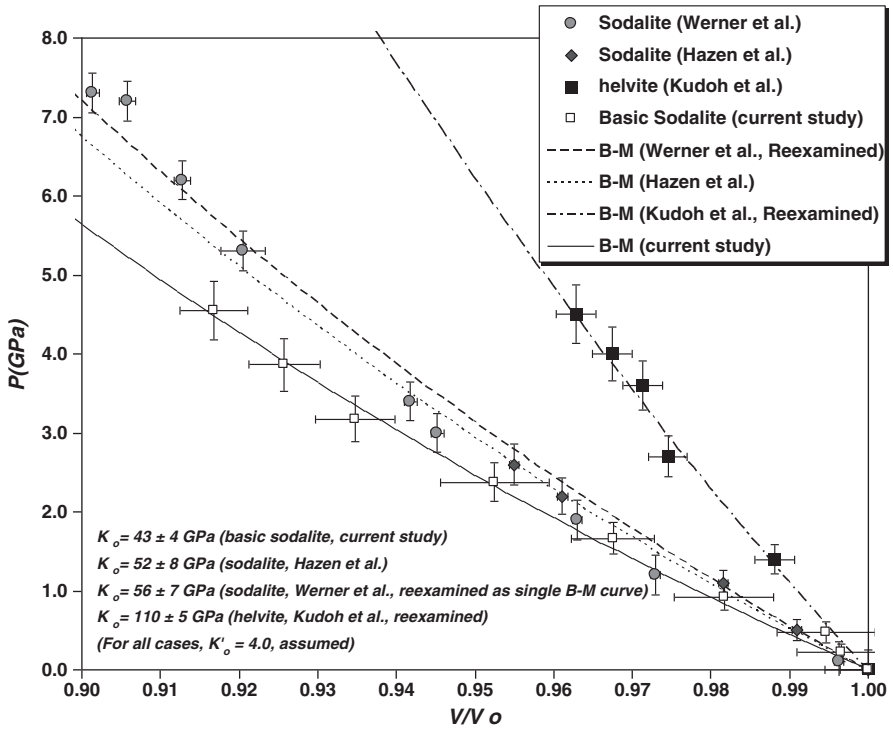


**Fig. 6.** Comparison of pressure-normalized volume data between sodalite and the basic sodalite. In this plot, sodalite appears more incompressible than the basic sodalite.

phase transition or peculiar compression behavior of the basic sodalite was observed up to 4.5 GPa. A comparison between the earlier high pressure studies and this study on sodalite framework zeolites (e.g., sodalite and helvite) indicates the following results: (1) the basic sodalite structure seems more flexible to external pressure than sodalite; this condition could be the result of two mechanisms: (a) the larger unit cell volume allows more flexible tilting of $AlO_4$ or $SiO_4$ tetrahedra or (b) the disordered characteristic of the guest molecules (i.e., $O_2H_3^-$) in the sodalite cage (the second mechanism implies that the bulk modulus of geopolymers may be modified by incorporating various guest ions by ion-exchange using different alkaline activators) and (2) the chemical composition of the framework structure is a more determining factor for the compressibility of sodalite framework zeolites than the topology of zeolite itself.

## Acknowledgments

This publication was based on work supported in part by Award No. KUS-l1-004021 made by the King Abdullah University of Science and Technology (KAUST) and the by NIST Grant 60NANB10D014. The work for the Advanced Light Source is supported by the Director, Office of Science, Office of Basic Energy Sciences, of the U.S. Department of Energy under Contract No. DE-AC02-05CH11231.

## References

[1] P.K. Mehta, P.J.M. Monteiro, Concrete: Microstructure, properties, and materials, McGraw-Hill, 2006.
[2] M. Ahmaruzzaman, A review on the utilization of fly ash, Prog. Energy Combust. Sci. 36 (2010) 327–363.
[3] N. Bouzoubaâ, B. Fournier, Optimization of fly ash content in concrete: Part I—Non-air-entrained concrete made without superplasticizer, Cem. Concr. Res. 33 (2003) 1029–1037.
[4] American Coal Ash Association (ACAA). Website: http://www.acaa-usa.org/.
[5] European Coal Combustion Products Association (ECOBA). Website: http://www.ecoba.com/.
[6] X. Querol, N. Moreno, J. Umana, A. Alastuey, E. Hernández, A. Lopez-Soler, F. Plana, Synthesis of zeolites from coal fly ash: An overview, Int. J. Coal Geol. 50 (2002) 413–423.
[7] J. Oh, P.J.M. Monteiro, S.S. Jun, S. Choi, S.M. Clark, The evolution of strength and crystalline phases for alkali-activated ground blast furnace slag and fly-ash-based geopolymers, Cem. Concr. Res. 40 (2010) 189–196.
[8] J.G.S. van Jaarsveld, J.S.J. van Deventer, L. Lorenzen, The potential use of geopolymeric materials to immobilise toxic metals: Part I—Theory and applications, Miner. Eng. 10 (1997) 659–669.
[9] A. Palomo, M.W. Grutzeck, M.T. Blanco, Alkali-activated fly ashes: A cement for the future, Cem. Concr. Res. 29 (1999) 1323–1329.
[10] Á. Palomo, S. Alonso, A. Fernandez-Jiménez, I. Sobrados, J. Sanz, Alkaline activation of fly ashes: NMR study of the reaction products, J. Am. Ceram. Soc. 87 (2004) 1141–1145.
[11] P. Duxson, A. Fernández-Jiménez, J.L. Provis, G.C. Lukey, A. Palomo, J.S.J. van Deventer, Geopolymer technology: The current state of the art, J. Mater. Sci. 42 (2007) 2917–2933.
[12] J.L. Provis, G.C. Lukey, J.S.J. van Deventer, Do geopolymers actually contain nanocrystalline zeolites? A reexamination of existing results, Chem. Mater. 17 (2005) 3075–3085.
[13] A. Fernández-Jiménez, A. Palomo, I. Sobrados, J. Sanz, The role played by the reactive alumina content in the alkaline activation of fly ashes, Microporous Mesoporous Mater. 91 (2006) 111–119.
[14] E. Bonaccorsi, S. Merlino, Modular microporous minerals: Cancrinite-davyne group and C–S–H phases, Rev. Min. Geochem. 57 (2005) 241–290.
[15] P.V. Krivenko, G.Yu. Kovalchuk, Heat-resistant fly-ash-based geocements, Proceedings of the Int. Conf. Geopolymer 28th–29th October 2002, Melbourne, Australia, 2002.
[16] M. Criado, A. Palomo, A. Fernández-Jiménez, Alkali activation of fly ashes: Part 1—Effect of curing conditions on the carbonation of the reaction products, Fuel 84 (2005) 2048–2054.
[17] T. Bakharev, Durability of geopolymer materials in sodium and magnesium sulfate solutions, Cem. Concr. Res. 35 (2005) 1233–1246.
[18] T. Bakharev, Geopolymeric materials prepared using class F fly ash and elevated temperature curing, Cem. Concr. Res. 35 (2005) 1224–1232.
[19] A. Fernandez-Jimenez, A. Palomo, M. Criado, Microstructure development of alkali-activated fly ash cement: A descriptive model, Cem. Concr. Res. 35 (2005) 1204–1209.
[20] T. Bakharev, Thermal behaviour of geopolymers prepared using class F fly ash and elevated temperature curing, Cem. Concr. Res. 36 (2006) 1134–1147.
[21] M. Criado, A. Fernández-Jiménez, A.G. de la Torre, M.A.G. Aranda, A. Palomo, An XRD study of the effect of the SiO2/Na2O ratio on the alkali activation of fly ash, Cem. Concr. Res. 37 (2007) 671–679.
[22] K. Dombrowski, A. Buchwald, M.J. Weil, The influence of calcium content on the structure and thermal performance of fly-ash-based geopolymers, J. Mater. Sci. 42 (2007) 3033–3043.
[23] A. Fernández-Jiménez, I. García-Lodeiro, A.J. Palomo, Durability of alkali-activated fly ash cementitious materials, J. Mater. Sci. 42 (2007) 3055–3065.
[24] E. Alvarez-Ayuso, X. Querol, F. Plana, A. Alastuey, N. Moreno, M. Izquierdo, O. Font, T. Moreno, S. Diez, E. Vazquez, M.J. Barra, Environmental, physical and structural characterisation of geopolymer matrixes synthesised from coal (co-) combustion fly ashes, J. Hazard. Mater. 154 (2008) 175–183.
[25] M. Wiebcke, G. Engelhardt, J. Felsche, P.B. Kempa, P. Sieger, J. Schefer, et al., Orientational disorder of the hydrogen dihydroxide anion,($O^2H^{3-}$) in sodium

hydroxosodalite dihydrate ($Na^8[Al^6Si^6O^{24}](OH)^2 \cdot 2H_2O$): Single-crystal X-ray and powder neutron diffraction and MAS NMR and FT IR spectroscopy, J. Phys. Chem. 96 (1992) 392–397.
[26] G. Engelhardt, J. Felsche, P. Sieger, The hydrosodalite system $Na_{6+x}[SiAlO_4]_6(OH)$. $nH_2O$: Formation, phase composition, and De- and rehydration studied by $^1H$, $^{23}Na$, and $^{29}Si$ MAS-NMR spectroscopy in tandem with thermal analysis, X-ray diffraction, and IR spectroscopy, J. Am. Chem. Soc. 114 (1992) 1173–1182.
[27] S. Luger, J. Felsche, P. Fischer, Structure of hydroxysodalite $Na_8[AlSiO_4]_6 \cdot (OH)_2$: A powder neutron diffraction study at 8 K, Acta Crystallogr., Sect. C: Cryst. Struct. Commun. 43 (1987) 1–3.
[28] I. Hassan, H.D. Grundy, Structure of basic sodalite, $Na_8Al_6Si_6O_{24}(OH)_2 \cdot 2H_2O$, Acta Crystallogr., Sect. C: Cryst. Struct. Commun. 39 (1983) 3–5.
[29] J. Felsche, S. Luger, C. Baerlocher, Crystal structures of the hydrosodalite $Na_6[AlSiO_4]_6 \cdot 8H_2O$ and of the anhydrous sodalite $Na_6[AlSiO_4]_6$, Zeolites 6 (1986) 367–372.
[30] M. Kunz, A. MacDowell, W. Caldwell, D. Cambie, R. Celestre, E. Domning, et al., A beamline for high-pressure studies at the Advanced Light Source with a superconducting bending magnet as the source, J. Synchrotron Radiat. 12 (2005) 650–658.
[31] A. P. Hammersley. Fit2d version 12.040, ESRF, Grenoble, France, 2006.
[32] R.W. Cheary, A.A. Coelho, Programs XFIT and FOURYA, deposited in CCP14 Powder Diffraction Library, Engineering and Physical Sciences Research Council, Daresbury Laboratory, Warrington, England, 1996 (http://www.ccp14.ac.uk/tutorial/xfit-95/xfit.htm).
[33] J. Laugier, and B. Bochu. CELREF. Version 3. Cell Parameter Refinement Program From Powder Diffraction Diagram. Laboratoire des Matériaux et du Génie Physique, Ecole Nationale Supérieure de Physique de Grenoble (INPG), France, 2002.
[34] H. Mao, J. Xu, P. Bell, Calibration of the ruby pressure gauge to 800 kbar under quasi-hydrostatic conditions, J. Geophys. Res. 91 (1986) 4673–4676.
[35] L. Lutterotti, S. Matthies, H. Wenk, MAUD (Material Analysis Using Diffraction): A User Friendly Java Program for Rietveld Texture Analysis and More, 1 (1999) 1599–1604. http://www.ing.unitn.it/maud/.
[36] W. Depmeier, Some examples of temperature and time resolved studies of the dehydration and hydration behavior of zeolites and clathrates, Part. Part. Syst. Char. 26 (2009) 138–150.
[37] F. Birch, Finite strain isotherm and velocities for single-crystal and polycrystalline NaCl at high pressures and 300 K, J. Geophys. Res. 83 (1978) 1257–1268.
[38] C. Meade, R. Jeanloz, Static compression of $Ca(OH)_2$ at room temperature: Observations of amorphization and equation of state measurements to 10.7 GPa, Geophys. Res. Lett. 17 (1990) 1157–1160.
[39] R. Jeanloz, Finite-strain equation of state for high-pressure phases, Geophys. Res. Lett. 8 (1981) 1219–1222.
[40] B.C. Reed, Linear least-squares fits with errors in both coordinates: II—Comments on parameter variances, Am. J. Phys. 60 (1992) 59–62.
[41] E. Knittle, Static compression measurements of equations of state, in: T. Ahrens (Ed.), Mineral Physics and Crystallography: A Handbook of Physical Constants. American Geophysical Union, 1995, pp. 184–209.
[42] G.D. Gatta, Does porous mean soft? On the elastic behaviour and structural evolution of zeolites under pressure, Z. Kristallogr. 223 (2008) 160–170.
[43] R.M. Hazen, Z.D. Sharp, Compressibility of sodalite and scapolite, Am. Mineral. 73 (1988) 1120–1122.
[44] S. Werner, S. Barth, R. Jordan, H. Schulz, Single crystal study of sodalite at high pressure, Z. Kristallogr. 211 (1996) 158–162.
[45] S.E. Latturner, J. Sachleben, B.B. Iversen, J. Hanson, G.D. Stucky, Covalent guest–framework interactions in heavy metal sodalites: Structure and properties of thallium and silver sodalite, J. Phys. Chem. B 103 (1999) 7135–7144.
[46] I. Hassan, H.D. Grundy, The crystal structures of sodalite-group minerals, Acta Crystallogr., Sect. B: Struct. Sci 40 (1984) 6–13.
[47] Y. Kudoh, Y. Takéuchi, The effect of pressure on helvite $Mn_8S_2[Be_6Si_6O_{24}]$, Z. Kristallogr. 173 (1985) 305–312.